metals

MDPI

Article

Effects of WC Particle Types on the Microstructures and Properties of WC-Reinforced Ni60 Composite Coatings Produced by Laser Cladding

Pengxian Zhang [1,*], Yibin Pang [1,2] and Mingwei Yu [1,2]

[1] State Key Laboratory of Advanced Processing and Recycling of Nonferrous Metals, Lanzhou University of Technology, Lanzhou 730050, China; Pangyibin1995@163.com (Y.P.); 432087187@139.com (M.Y.)

[2] Wenzhou Pump and Valve Engineering Research Institute, Lanzhou University of Technology, Wenzhou 325024, China

* Correspondence: pengxzhang@163.com; Tel.: +86-139-931-95279

Received: 21 April 2019; Accepted: 19 May 2019; Published: 21 May 2019

Abstract: WC-reinforced Ni60 composite coatings with different types of WC particles were prepared on 304 stainless steel surface by laser cladding. The influences of spherical WC, shaped WC, and flocculent WC on the microstructures and properties of composite coatings were investigated. The results showed that three types of WC particles distribute differently in the cladding coatings, with spherical WC particles stacking at the bottom, shaped WC aggregating at middle and lower parts, with flocculent WC particles dispersing homogeneously. The hardnesses, wear resistances, corrosion resistances, and thermal shock resistances of the coatings are significantly improved compared with the stainless steel substrate, regardless of the type of WC that is added, and especially with regard to the microhardness of the cladding coating; the addition of spherical or shaped WC particles can be up to 2000 $HV_{0.05}$ in some areas. Flocculent WC, shaped WC, and spherical WC demonstrate large to small improvements in that order. From the results mentioned above, the addition of flocculent WC can produce a cladding coating with a uniform distribution of WC that is of higher quality compared with those from spherical WC and shaped WC.

Keywords: laser cladding; Ni60-WC; three types of WC particles; particle distribution; microstructures and properties

1. Introduction

Laser cladding, an advanced form of surface modification technology, has been widely used in various fields over recent years. The cladding material plays an important role in the performance of the cladding coating. Among them, Ni-based self-fusible alloy powder, which is a common cladding material, has been most widely studied and applied as laser cladding material, for its good wear resistance and corrosion resistance [1]. However, the wear resistances of Ni-based cladding materials cannot meet the stringent operating requirements for valves, axles, and other parts that are used under harsh working conditions. WC is an ideal hard-phase material in the cladding coating, due to its high level of hardness, high wear resistance, and good wettability with Ni-based alloys, and it has been extensively used as a reinforcement in Ni-based alloys, to enhance the wear resistance of materials [2–4]. The influences of laser power, cladding speed and WC content on the microstructure and properties of the cladding coating were studied in the literature [5–9], and the melting crystallization of WC particles and the influence mechanism on the wear resistance and corrosion resistance were discussed. However, owing to the obvious interface, and to factors including the large performance difference between the Ni-based alloy and the WC hard phase, the phenomenon of WC particles falling off, melting, burning, and sinking easily occurs during laser cladding. The WC particles deposited at the

bottom of the cladding coating are not conducive to the wear resistance of the cladding coating surface, and instead they can also cause abrupt changes in the properties of the matrix that are related to the cladding coating, which easily lead to cracks and fatigue damage, and these are some of the biggest obstacles to their engineering applications [10,11].

The melting of the WC particles and the re-precipitation of the carbides have the effect of dispersing the hardened cladding coating, and the uniform distribution of the WC particles on the surface of the cladding layer can significantly improve the wear resistance of the cladding coating [12]. However, it is difficult to prepare a WC-reinforced composite coating with a uniform distribution, due to the different densities of the metal matrix and the WC particles. Mechanical vibration, ultrasonic, magnetic fields, and other auxiliary methods [13–15] can be used to control the microstructural evolution of ceramic-reinforced composite coatings, so as to achieve a uniform distribution of ceramic particles in the composite coating. However, it is still difficult to implement practical industrial applications for these methods, owing to the shortcomings of the equipment and the environmental constraints. In addition, the distribution of the WC in the cladding coating is closely related to the size and shape of WC. Selecting WC particles with similar properties and good wettabilities by using Ni-based alloys can solve the problem of WC particles falling off and sinking into the cladding coating [16,17]. Compared with external auxiliary methods, the influences of different WC particles on the microstructures and properties of the cladding coating are revealed by changing the types of WC particles, so as to obtain a high-quality cladding coating with a uniform WC distribution, which is more applicable for industrial use. So far, scholars at home and abroad have conducted much in-depth research on the influencing mechanisms of the microstructures and properties of the cladding coating that result from the addition of specific types of WC particles [18–20], but the influencing mechanisms of different types of WC particles on the microstructures and properties of cladding coatings have been rarely reported. For this reason, Ni/WC composite coatings were produced on the surface of a 304 stainless steel substrate by laser cladding technology in this paper. The objective was to add floccus WC, spherical WC, or shaped WC, in order to conduct comparative experiments, and to determine the microstructure, wear resistance, corrosion resistance, and thermal shock resistance of the cladding coating as evaluation indexes. In so doing, the influences of WC particle types on the microstructure and performance of the cladding coating would be studied, to explore the formation mechanism of a high quality cladding coating with a uniform WC distribution.

2. Materials and Experimental Procedure

In this experiment, a stainless steel 304 with dimensions of 100 mm × 65 mm× 10 mm was used as the substrate; the surface was ground with sandpaper to remove the oxide layer, and washed with absolute ethanol. The composition of 304 stainless steel is shown in Table 1. The clad materials used in this study were Ni60 (see Table 2)/WC composite powders, in which the size range of the Ni60 powder particles was in the range of 140–325 mesh. Three types of WC particles were added: spherical WC with a particle size of −100/+325 mesh; shaped WC with a particle size of −100/+325 mesh; flocculent WC with a particle size of particle size −325 mesh, and WC12Co powder. Figure 1 presents scanning electron microscopy (SEM) images of the composite powders with the addition of spherical WC powder, shaped WC powder, and flocculent WC powder. Three kinds of WC powders were fully and uniformly mixed with the Ni60 powders at a mass ratio of 30%, using a ball mill (a rotating speed of 120 r/min and a mixing time of 3 h).

Table 1. Chemical composition of stainless steel (wt %).

S	P	C	Si	Mn	Ni	Cr	Fe
0.03	0.045	0.07–0.08	0.075–1	2	8–11	18–20	Bal.

Table 2. Chemical composition of Ni60 powder (wt %).

C	W	B	Si	Fe	Cr	Ni
0.80	3.00	3.50	4.00	15.00	15.00	Bal

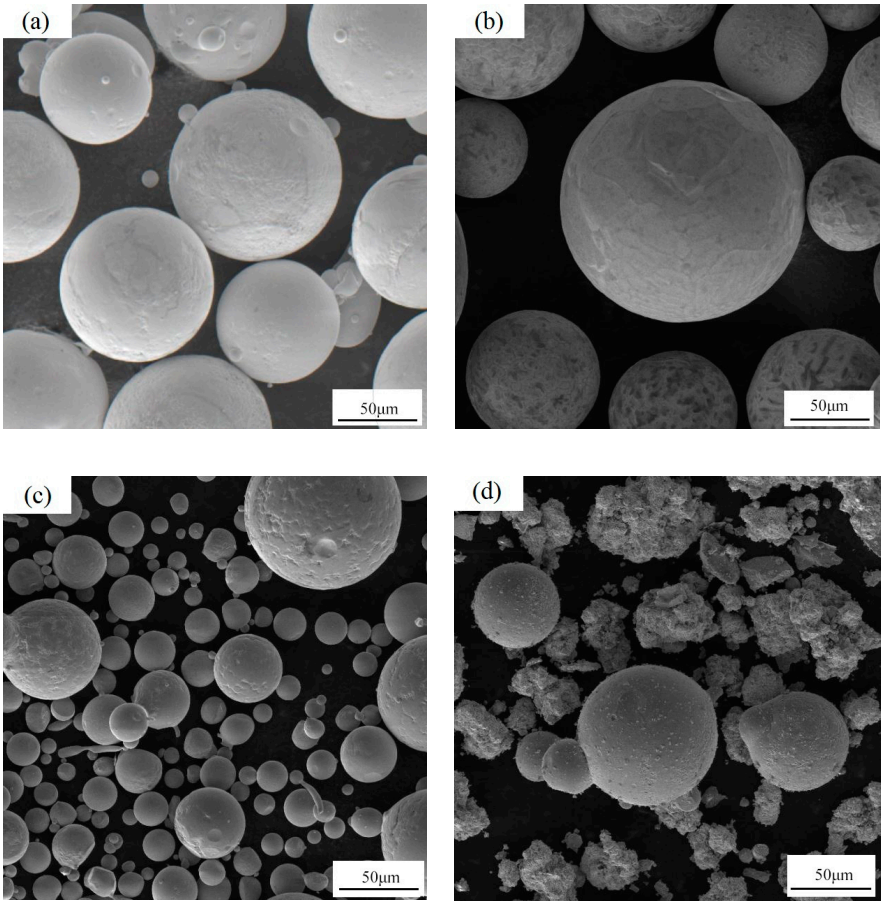

Figure 1. Scanning electron microscopy (SEM) images of (**a**) Ni60, (**b**) Ni60-spherical WC, (**c**) Ni60-shaped WC and (**d**) Ni60-flocculent WC.

The stainless steel sample was preheated to 500 °C (with the aim of reducing crack sensitivity) before the test, and laser cladding was performed, using a FL-DLight 3S-2000-type semiconductor laser (Juguang, Xi'an, China) and a five-axis numerical control system. Composite powders were conveyed by a coaxial-powder feeding technology, while 99.9% pure argon with a flow rate of 10 L/min was used as the protective gas. The processing parameters of the cladding layer were as follows: a laser power of 1.5 kW, a laser scanning speed of 240 mm/min, a powder feeding rate of 7 r/min, a spot size of 4 × 5 mm, and an overlapping rate of 40%. After laser cladding, the specimens were cooled in air at room temperature, to reduce the probability of cracking.

After polishing and cleaning, the cross-sectional samples were etched chemically in the erosion solution ($CuSO_4 \cdot 5H_2O$:HCl:H_2O = 16:50:434) to reveal the microstructure of the coating. For microstructure characterization, the composite coatings were analyzed with a metallographic microscope (lmager.M2m, ZEISS, Heidenheim, Germany) and a scanning electron microscope equipped with an energy-dispersive spectrometer (LYRA3, TESCAN ORSAY HOLDING, Shanghai, China). The microhardnesses of the samples were measured by a MVC-1000JMT1 microhardness tester (Huike, Tianjin, China) with a load of 50 N and a dwelling time of 15 s along the clad height. The reversal dry sliding wear tests were performed using a CFT-I wear tester (Kaihua, Lanzhou, China), with a ball-on disk configuration. The friction pair was a ceramic ball with a diameter of 5 mm. The tribological

tests were carried out under applied loads of 30 N, rated at 800 r/min and 60 min application time in air. After the wear test, the wear widths of the wear scars were measured as non-contact surface roughness, using a TAL YSURF CLI 1000 instrument (Taylor Hobson, Shanghai, China). Formulas (1) and (2) are used to calculate the volume wear rate of the sample, and to evaluate the wear resistance of the cladding layer [21]:

$$\Delta V = L_0\left(r^2 \arcsin\frac{b}{2r} - \frac{b}{2}\sqrt{r^2 - \frac{b^2}{4}}\right) \quad (1)$$

where ΔV refers to the wear volume, L_0 refers to the circumference of the wear scar, r refers to the radius of the steel ball, and b refers to the width of the wear scar.

$$w = \frac{\Delta V}{N \cdot L} \quad (2)$$

where w refers to the wear rate of the coating, N refers to the load, and L is the total reciprocating distance of the run.

Electrochemical tests were conducted in 3.5 wt % NaCl solution with an electrochemical working station (CHI 660E, Shanghai, China). A three-electrode cell setup, which was composed of a working electrode made from the coating sample with an exposed area of 1 cm^2, a saturated calomel electrode, and a Ag/AgCl electrode as the reference, was used for the electrochemical measurement. The potentiodynamic polarization curves were recorded at a scanning rate of 0.01 V/s over a voltage scanning range from −3 V to +1.2 V. The thermal shock test was performed with a cladding coating block with dimensions of 20 mm × 20 mm, which was polished to test the adhesion of the coating. According to the JISH86662199 industrial standard in Japan, the thermal shock test was carried out by the water quenching method. After holding the sample at 800 °C in a furnace for 20 min, the sample is immediately transferred to room temperature water to be cooled. When the temperature of the sample is the same as that of the water, the sample is again placed into the furnace for heat preservation. The above describes a thermal shock cycle; after that, the thermal shock experiments are repeated, to record the extent of cracking on the surface of the sample, in order to evaluate the bonding properties of the coating [22].

3. Results

3.1. Microstructures of the Coatings

Under the same process parameters as above, the cross-sectional micrographs of the cladding coatings with different types of WC are shown in Figure 2a,c,e. It was seen that the overall shapes of the cladding coatings are regular, the interfaces of the cladding coating near the 304 substrate are relatively flat with no cracks, a small number of pores can observed through the cladding coating, and the morphologies and distributions of different types of WC are significantly different. The spherical WC particles are regular spheres with diameters ranging from 45 to 150 μm, mainly distributed in the lower part of the cladding coating, and only a small amount of smaller particles are present in the upper and middle parts of the cladding coating. The shaped WC particles are irregular polyhedrons, which are mainly distributed in the middle and lower parts of the cladding coating, and they are sparsely distributed on the surface of the cladding layer. The measurements show that the long diameters are less than 150 μm, and that the short diameters are between 20 and 70 μm for the shaped WC particles. The flocculent WC particles are a spatial cotton-like structure with a particle diameter of less than 45 μm. It can be seen from Figure 2e that the particles are evenly distributed at various positions of the cladding coating, and that there is no significant relationship between the particle size and the distribution position. In the process of the laser cladding, the main reasons for the above significant differences are as follows:

(1) The melting point and density of the WC particles are higher than those of the Ni-based cladding alloy. With a melted Ni-based alloy to form a liquid molten pool, the WC remained in a complete particle state.

(2) Intense convection caused by laser shock, and the stirring of the molten pool during laser cladding, can cause the WC particles to be evenly distributed through all positions of the molten pool.

(3) During the process of cooling and solidification of the molten pool, WC particles tend to precipitate at the bottom of the molten pool, as the stirring action of the molten pool slows down. Among the three kinds of WC particles, a spherical WC particle has the largest size and the heaviest weight, so that the precipitation phenomenon is the most obvious. The flocculent WC particles are very small in size, with the existence of a large number of interspace structures, reducing the density of the unit volume. Therefore, the flocculent WC is evenly distributed in the cladding coating without precipitation.

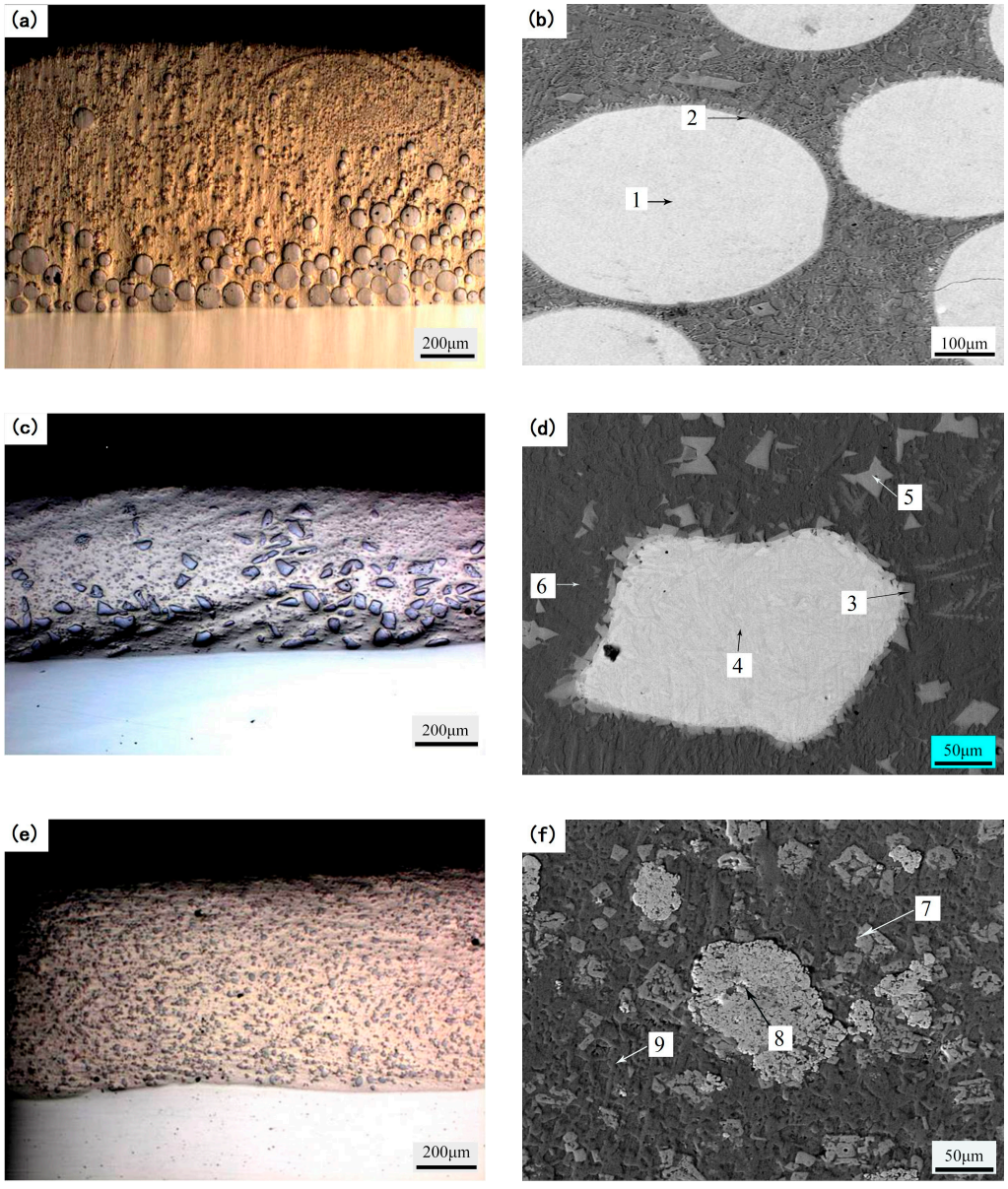

Figure 2. Metallographic microscopy and SEM images of cladding coatings with different types of WC. Metallographic microscopes of (**a**) Ni60-spherical WC, (**c**) Ni60-shaped WC, and (**e**) Ni60-flocculent WC, and SEM photos of (**b**) Ni60-spherical WC, (**d**) Ni60-shaped WC, and (**f**) Ni60-flocculent WC.

The SEM photos of the three different types of WC particles are shown in Figure 2b,d,f, and the scanning electron microscope equipped with an energy-dispersive spectrometer (EDS) analysis results corresponding to different positions in the figure were listed in Table 3. It can be observed from the figure that the spherical WC and the shaped WC generally maintained their original morphologies and sizes, indicating that the WC particles were less soluble under the process parameters of the experiment. The analyses of points 1 and 4 showed that the compositions of any two WC particles were substantially the same, being mainly composed of WC and W_2C. A slew of irregular needle-like or block-like gray phases were generated at the edges, and at the adjacent substrates of the spherical WC and the shaped WC particles, as shown in points 2, 3, and 5 in the figure. EDS results showed that the components of the gray phases were roughly the same, all of these were compounds that were rich in C, Cr, Fe, and W. Studies have shown that these compounds pertain to the hard phases of carbides such as $M_{23}C_6$, M_7C_3, and M_6C. Points 6 and 9, containing large amounts of Ni and Fe, were mainly composed of γ-(Ni,Fe) phases, which belonged to a face-centered cubic structure. The reason for these phenomena is that during the laser cladding process, the laser energy causes a partial melting of the WC particles, and the C and W elements combine with Cr, Fe, and Ni to form the complex carbides $M_{23}C_6$, M_7C_3, and M_6C, which distribute in the matrix to form needle-like or block-like gray phases. When the WC particles are heated, the C and W elements on the surface diffuse with the substrate elements of the cladding coating, forming a diffusion layer with a certain degree of thickness. During the cooling process, recrystallization generates irregular M_xC_y phases surrounding the surface of the WC particles.

Table 3. The scanning electron microscope equipped with an energy-dispersive spectrometer (EDS) analysis results of the cladding coating.

Point	W	Fe	Cr	Ni	B	Si	C	Co
1	61.2	-	-	-	-	-	38.8	-
2	15.9	8.6	26.8	6.4	8.5	-	33.8	-
3	16.4	8.9	26.5	7.5	6.4	-	34.2	-
4	57.7	-	-	-	-	-	42.3	-
5	16.2	8.6	28.5	7.0	7.4	-	34.6	-
6	0.8	18.2	7.6	58.3	-	4.6	10.5	-
7	14.5	12.2	8.4	23.2	-	0.8	38.3	2.6
8	18.7	9.7	12.0	14.1	-	-	43.6	1.9
9	1.2	17.3	14.3	49.2	-	3.1	14.8	-

The microstructure of the cladding coating with flocculent WC particles was obviously different from those of the other two kinds of structures. As can be seen from Figure 2, flocculent WC particles were fine and dispersed within the cladding layer, and there were many small WC particles with diameters of less than 10 μm in the structure. The edges of the flocculent WC did not have M_xC_y gray phases, of which the morphologies in the matrix were mostly fine-block or flocculent, with a particle size of less than 10 μm. The EDS analysis showed that the gray phases had the same compositions as the M_xC_y phases on the surfaces of the other two WC particles, but they contained more Ni elements. This was because the original unit sizes of the flocculent WC particles were small, forming a space–cotton flocculent structure via the accumulation of nano-sized WC particles. This structure was relatively loose and easily to collapsed under the impact of the laser energy and the agitation of the molten pool. The outer layers of the WC particles melt under the thermal action of the laser, so that free W and C elements recrystallize with Cr, Fe, and Ni to form massive carbides. After the collapse, the elements of the smaller flocculent WC particles and the cladding coating diffuse with each other, and the diffusion acts upon all the WC particles to form the flocculent carbide structures, as in point 7 in Figure 2f.

3.2. Microhardness of Coatings

Under the same process parameters, the microhardness profiles of the laser-clad coatings obtained by adding Ni60 powder and different types of WC powders are shown in Figure 3, which shows a certain degree of variation from the surfaces of the coatings to the substrate. The average microhardnesses of the cladding coatings of the four materials were greater than 500 $HV_{0.05}$, which was approximately 2.5-fold higher than that of the 304 stainless steel substrate. The microhardness of the heat-affected zone between the cladding coating and the substrate decreased rapidly until it reached the hardness of the substrate (210 $HV_{0.05}$). The microhardnesses of most points with each cladding coating were within a range of 600~1000 $HV_{0.05}$, indicating that the addition of different types of WC particles had little influence on the hardness of the Ni60 cladding coating. There were a few points in each cladding coating where the microhardness ranged from 1000 to 1400 $HV_{0.05}$. Studies have shown that these points contain M_xC_y carbides. The microhardnesses of the cladding coatings with spherical and shaped WC particles had obvious peak values, which reached up to 1600–2000 $HV_{0.05}$, mainly due to mutual diffusion between the hard phase and the substrate, dispersion strengthening of the fine carbides, strengthening of the hard phase, solid-solution strengthening of alloying elements such as C, Cr, Ni, and W, and the interface strengthening of the hard phase and the substrate. However, the microhardnesses of the WC particles in the cladding coating with the addition of the flocculent WC were only about 1000 $HV_{0.05}$, and these were determined by the sizes and spatial morphologies of the flocculent WC particles. Both the flocculent WC particles with sizes of less than 45 μm and the diffused M_xC_y hard phase had many "pores" filled with γ-Ni, resulting in a reduced supporting effect by WC on the cladding coating, which was reflected in the decrease of microhardness.

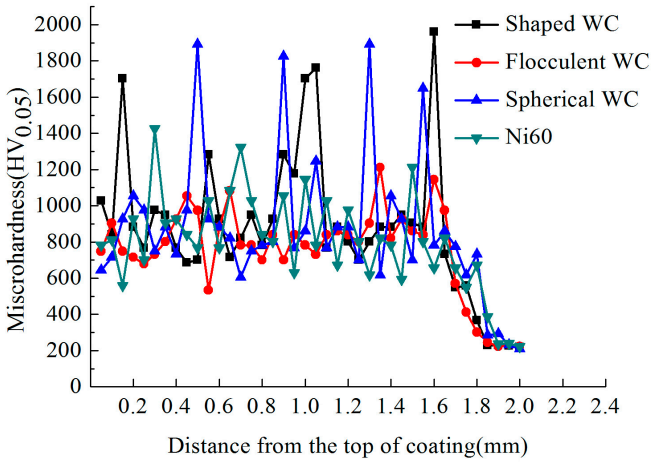

Figure 3. Microhardness distribution of the cladding coating.

3.3. Wear Behaviors of Coatings

Figure 4 shows the wear curves of the Ni60 coatings with different types of WC particles. It can be seen that the average wear coefficient of Ni60 coating without WC was 0.5, whereas the average abrasion coefficients of the Ni60 coating with 30 wt % flocculent WC, shaped WC, or spherical WC, were 0.4, 0.35, and 0.2, respectively, which were significantly lower values than that of the Ni60 cladding coating. From the curve amplitude, the curve amplitude of Ni60 + 30 wt % flocculent WC sample was larger, while the vibration amplitudes of the other two coatings with WC were small.

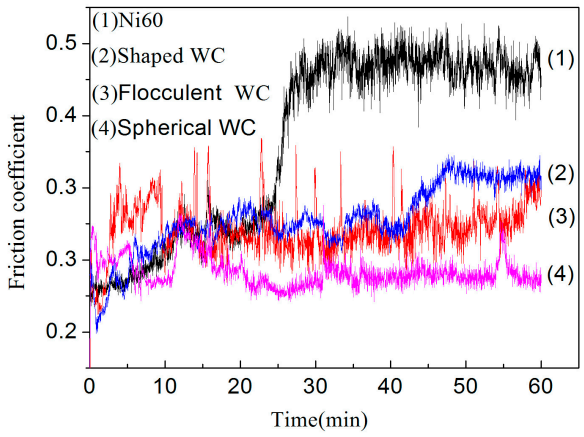

Figure 4. Friction coefficient curve of the cladding coating.

Figure 5 shows the volume wear rates of the coatings. Comparing the wear rates of the four coatings, it can be found that compared with the Ni60 cladding coating, the wear rates of the cladding coatings with the addition of the three kinds of WC particles were significantly decreased, among which the coatings with spherical WC added had the highest wear rates, while the coating with the flocculent WC added had the lowest wear rates. The possible reason for this was that the hardnesses of the WC particles were more than 1500 $HV_{0.05}$, which were approximately two-fold higher than that of the average hardness of the Ni60 cladding coating. When friction and wear occur in the cladding coating, hard WC particles play a very good supporting role for the substrate, and the WC particles and matrixes play roles in resisting micro-cutting, which can significantly reduce the surface wear.

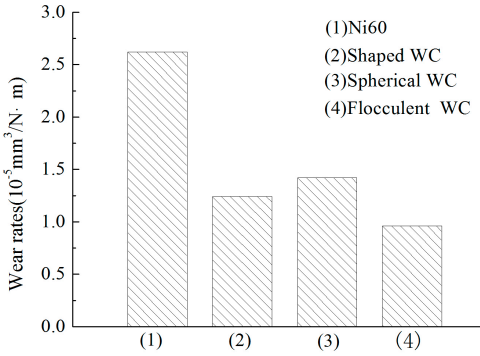

Figure 5. The volume wear rates of the cladding coating.

The surface morphologies of the coatings after wearing are illustrated in Figure 6. There was a small amount of WC on the surface of the cladding coating with the spherical WC added, which resulted in most of the wear marks being present on the Ni60 matrix, so that the relative wear rates for this sample were the largest. On the one hand, the cladding coating with flocculent WC has a uniform supporting effect on the entire wear scar, due to the uniform distribution of a large number of fine flocculent WC particles on the surface; on the other hand, the flocculent WC is well-combined with the matrix, due to its interaction with the substrate, and the smaller sizes of the floccus WC particles are able to reduce the stress concentration. Therefore, the wear rates of the coating with the flocculent WC particles are the lowest.

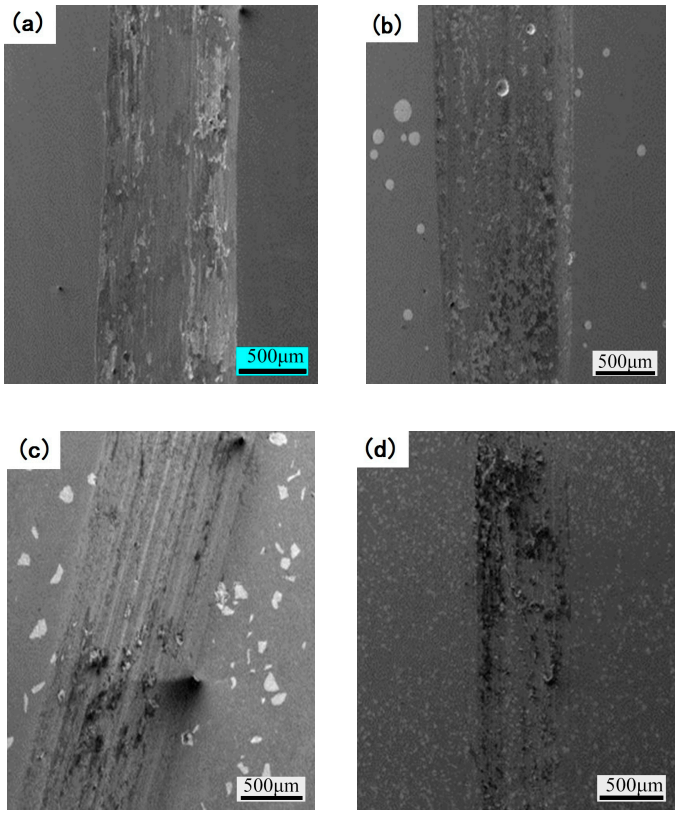

Figure 6. SEM images of the worn surfaces of different coatings. (**a**) Ni60, (**b**) Ni60-spherical WC, (**c**) Ni60-shaped WC, (**d**) Ni60-flocculent WC.

3.4. Electrochemical Corrosion of Coatings

Figure 7 shows the electrochemical polarization curves of the composite coatings with the three types of WC particles in 3.5 wt % NaCl solution. The electrochemical properties of the cladding coatings were analyzed by comparing the Tafel polarization curves. The analysis showed that the corrosion potential of the composite coating with the addition of spherical WC particles was −0.35 V, of which the corrosion current density was 0.538 A/m^2. The corrosion potential of the composite coating with shaped WC particles added, was −0.29 V, of which the corrosion current density was 0.577 A/m^2. The corrosion potential of the composite coating, with flocculent WC added, was −0.21 V, of which the corrosion current density was 0.491 A/m^2.

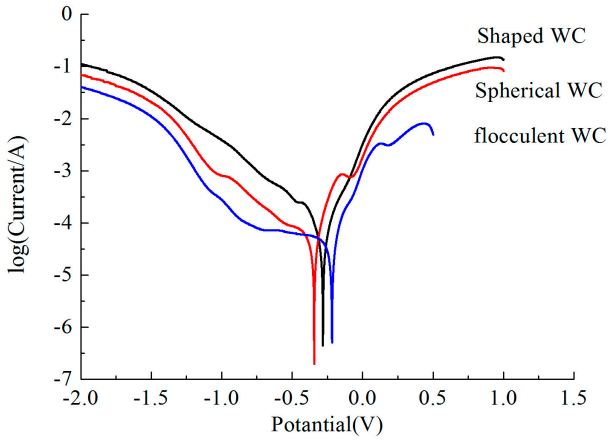

Figure 7. Electrochemical polarization curves of three types of WC cladding coatings.

It can be seen from the above results that the absolute values of corrosion potential of the three kinds of cladding coatings were spherical WC, shaped WC, and flocculent WC, respectively, from the largest to the smallest, indicating that the cladding coating with spherical WC added was the first to be corroded, and that the cladding coating with flocculent WC added was the last to be corroded when electrochemical corrosion occurred. It is generally believed that a lower corrosion current density denotes a lower corrosion rate. That is to say, the corrosion rate of a cladding coating with spherical WC added was the highest, while that of a cladding coating with flocculent WC added was the lowest. Compared with the spherical and shaped WC particles, the interface between the flocculent WC particles and the Ni60 matrix was more strongly dissolved and diffused, resulting in intense metallurgical bonding and a strong chemical affinity between the WC particles and Ni60 matrix, thus enhancing the stability of the composite coating. In addition, there was a lower number of unmelted flocculent WC particles in the composite coating, which led to the number of galvanic cells being correspondingly reduced. In summary, the corrosion resistance of the cladding coating with flocculent WC added was significantly better than the resistances of the other two materials.

3.5. Associativity

The thermal shock test was selected as a means to test the bonding strength of the cladding coating, and the test results are shown in Table 4. This thermal shock experiment was conducted 100 times, and only the shaped WC sample generated 1 × 1 mm spalling at the corner. The observation of the sample showed that the spalling surface was at the lower part of the cladding coating, rather than at the bonding surface, indicating that the laser cladding coating and the matrix were firmly metallurgically bonded, rather than simple mechanical bonding. In this paper, the criteria for the failure of the thermal shock samples were as follows: A. Cracks appear on the surfaces of the sample; B. The crack rate of the sample reaches 5%; C. All surfaces of the sample are cracked. The test results showed that the thermal shock resistance of the coating with flocculent WC added was significantly better than the other two. This is because WC is a hard and brittle material, and it has a different thermal expansion coefficient to Ni-based alloys. During the thermal shock test, great thermal stress was generated; the WC in the cladding coating often could not tolerate this stress and cracked first, producing a crack source. The crack propagates along the WC to the Ni-based cladding coating, and it eventually spreads to the surface, forming macroscopic cracks that are visible to the naked eye. The unit sizes of the flocculent WC particles are small, and they can easily avoid thermal stress concentrations and reduce the cracking tendency of the cladding coating. Relatively speaking, the unit sizes of the spherical WC and the shaped WC can reach 150 μm, and these have obvious effects on the fracture of matrix structure. Therefore, the thermal shock resistance of a sample with two kinds of WC particles is significantly reduced, among which the shaped WC particles are more likely to have stress concentrations than the spherical WC, because of their many edges and corners. Accordingly, the thermal shock resistance of a coating with shaped WC added was the worst among the three types of WC particles.

Table 4. Results of the thermal shock test.

Test Times	Spherical WC	Shaped WC	Flocculent WC
Appearance of cracks	2	1	3
5% crack rate	3	2	14
Appearance of crazing on the entire surface	5	3	33
Appearance of spalling	-	30	-

4. Conclusions

Under the same laser cladding process conditions, it is found that the addition of different WC particles have different influences on different aspects of the performance of the Ni60 coating, as follows:

(1) The spherical WC are mostly distributed within the lower part of the structure, and the shaped WC particles are mainly stacked in the middle and lower parts, while the flocculent WC particles are basically dispersed homogeneously in various positions. Both the surfaces and the substrates of the coating, with the addition of either spherical WC or shaped WC, had needle-like or block-like hard phases (M_xC_y), while the addition of flocculent WC only produced flocculent and block-like hard phases in the substrate of the cladding coating.

(2) The microhardnesses of the coatings with added spherical WC or shaped WC are relatively higher than the microhardnesses of the Ni60 coating and substrate. On the contrary, the microhardness of the cladding coating with flocculent WC added is slightly lower than that of the Ni60 matrix. However, due to the uniform distribution of the flocculent WC particles in the cladding coating, and because of their smaller sizes, they can play a uniform supporting role in the cladding layer and reduce the degree of stress concentration; therefore, a cladding coating with added flocculent WC has a better degree of wear resistance.

(3) Electrochemical measurements and the thermal shock test indicated that the cladding coating with additional flocculent WC has a higher degree of corrosion resistance and associativity compared with the cladding coatings where spherical or shaped WC are added. In summary, the main reason for why the cladding coating with flocculent WC added has more favorable comprehensive properties than coatings with spherical WC or shaped WC added is due to the structure of the cladding coating, with flocculent WC particles distributed uniformly through the cladding layer in fine block-like and flocculent hard phases, and also due to the smaller sizes of the flocculent WC particles.

Author Contributions: Conceptualization, P.Z. and M.Y.; Data curation, Y.P. and M.Y.; Formal analysis, P.Z.; Funding acquisition, P.Z.; Investigation, P.Z. and M.Y.; Methodology, Y.P.; Project administration, P.Z.; Supervision, Y.P. and M.Y.; Writing—original draft, Y.P.; Writing—review & editing, P.Z. and Y.P.

Funding: This research received no external funding.

Acknowledgments: The authors gratefully acknowledge the financial support from Wenzhou pump and Valve Engineering Research Institute.

Conflicts of Interest: The authors declare no conflict of interest.

References

1. Moustafa, S.F.; Abdel-Hamid, Z.; Baheig, O.G.; Hussien, A. Synthesis of WC hard materials using coated powders. *Adv. Powder Technol.* **2011**, *22*, 596–601. [CrossRef]
2. Parisa, F.; Radovan, K. Corrosion and wear behavior of laser cladded Ni-WC coatings. *Surf. Coat. Technol.* **2015**, *276*, 121–135.
3. St-Georges, L. Development and characterization of composite Ni-Cr + WC laser cladding. *Wear* **2007**, *263*, 562–566. [CrossRef]
4. Huang, B.; Xiong, W.; Yao, Z.; Chen, S.; Zhang, M.; Yang, Q. Effect of WC content on microstructure and mechanical properties of Ni_3Al-bonded cermets. *Ceram. Int.* **2016**, *42*, 5291–5298. [CrossRef]
5. Zhang, P.; Liu, Z. Physical-mechanical and electrochemical corrosion behaviors of additively manufactured Cr-Ni-based stainless steel formed by laser cladding. *Mater. Des.* **2016**, *100*, 254–262. [CrossRef]
6. Ma, Q.; Li, Y.; Wang, J.; Liu, K. Microstructure evolution and growth control of ceramic particles in wide-band laser clad Ni60/WC composite coatings. *Mater. Des.* **2016**, *92*, 897–905.
7. Farahmand, P.; Kovacevic, R. Laser cladding assisted with an induction heater (LCAIH) of Ni-60%WC coating. *J. Mater. Process. Technol.* **2015**, *222*, 244–258. [CrossRef]
8. Bartkowskin, D.; Mynarczak, A.; Piasecki, A.; Dudziak, B.; Gościański, M.; Bartkowska, A. Microstructure, microhardness and corrosion resistance of Stellite-6 coatings reinforced with WC particles using laser cladding. *Opt. Lasers Eng.* **2015**, *68*, 191–201. [CrossRef]
9. Ma, Q.; Li, Y.; Wang, J.; Liu, K. Investigation on cored-eutectic structure in Ni60/WC composite coatings fabricated by wide-band laser cladding. *J. Alloys Compd.* **2015**, *645*, 151–157. [CrossRef]

10. Alidokht, S.A.; Yue, S.; Chromik, R.R. Effect of WC morphology on dry sliding wear behavior of cold-sprayed Ni-WC composite coatings. *Surf. Coat. Technol.* **2019**, *357*, 849–863. [CrossRef]
11. Chong, P.; Man, H.; Yue, T. Microstructure and wear properties of laser surface-cladded Mo-WC MMC on AA6061 aluminum alloy. *Surf. Coat. Technol.* **2001**, *145*, 51–59. [CrossRef]
12. Yao, J.; Zhang, J.; Wu, G.; Wang, L.; Liu, R. Microstructure and wear resistance of laser cladded composite coatings prepared from pre-alloyed WC-NiCrMo powder with different laser spots. *Opt. Lasers Eng.* **2018**, *101*, 520–530. [CrossRef]
13. Liu, H.; Xu, Q.; Wang, C.; Zhang, X. Corrosion and wear behavior of Ni60CuMoW coatings fabricated by combination of laser cladding and mechanical vibration processing. *J. Alloys Compd.* **2015**, *621*, 357–363. [CrossRef]
14. Li, M.; Han, B.; Wang, Y.; Song, L.; Guo, L. Investigation on laser cladding high-hardness nano-ceramic coating assisted by ultrasonic vibration processing. *Optik* **2016**, *127*, 4596–4600. [CrossRef]
15. Wang, L.; Yao, J.H.; Hu, Y.; Zhang, Q.L.; Sun, Z.; Liu, R. Influence of electric-magnetic compound field on the WC particles distribution in laser melt injection. *Surf. Coat. Technol.* **2017**, *315*, 32–43. [CrossRef]
16. Sundaramoorthy, R.; Tong, S.X.; Parekh, D.; Subramanian, C. Effect of matrix chemistry and WC types on the performance of Ni-WC based MMC overlays deposited by plasma transferred arc (PTA) welding. *Wear* **2017**, *376*, 1720–1727. [CrossRef]
17. Guo, C.; Chen, J.M.; Zhou, J.S.; Zhao, J.R.; Wang, L.Q.; Yu, Y.J.; Zhou, H.D. Effects of WC–Ni content on microstructure and wear resistance of laser cladding Ni-based alloys coating. *Surf. Coat. Technol.* **2012**, *206*, 2064–2071. [CrossRef]
18. Erfanmanesh, M.; Abdollah-Pour, H.; Mohammadian-Semnani, H.; Shoja-Razavi, R. Kinetics and oxidation behavior of laser clad WC-Co and Ni/WC-Co coatings. *Ceram. Int.* **2018**, *44*, 12805–12814. [CrossRef]
19. Ortiz, A.; García, A.; Cadenas, M.; Fernández, M.R.; Cuetos, J.M. WC particles distribution model in the cross-section of laser cladded NiCrBSi + WC coatings, for different wt% WC. *Surf. Coat. Technol.* **2017**, *324*, 298–306. [CrossRef]
20. Weng, Z.; Wang, A.; Wu, X.; Wang, Y.; Yang, Z. Wear resistance of diode laser-clad Ni/WC composite coatings at different temperatures. *Surf. Coat. Technol.* **2016**, *304*, 283–292. [CrossRef]
21. Zhang, J.; Hu, Y.; Tan, X.J.; Guo, L.; Zhang, Q. Microstructure and high temperature tribological behavior of laser cladding Ni60A alloys coatings on 45 steel substrate. *Trans. Nonferrous Met. Soc. China* **2015**, *25*, 1525–1532. [CrossRef]
22. Chen, X.; Zhang, L.; Wang, M.Z.; Chen, Y.C.; Wang, H.T.; Bai, X.B. Thermal shock property of thermal sprayed TiB2-50Ni cermet coatings. *Chin. J. R. Metal.* **2017**, *1*, 32–39.